IOPscience iopscience.iop.org

Home Search Collections Journals About Contact us My IOPscience

# Microstructural characterization of carbon films and $CN_x$ films produced by $N^+$ implantation

This article has been downloaded from IOPscience. Please scroll down to see the full text article.

1997 J. Phys.: Condens. Matter 9 1743

(http://iopscience.iop.org/0953-8984/9/8/007)

View the table of contents for this issue, or go to the journal homepage for more

Download details:
IP Address: 171.66.16.207
The article was downloaded on 14/05/2010 at 08:10

Please note that terms and conditions apply.

J. Phys.: Condens. Matter **9** (1997) 1743–1761. Printed in the UK PII: S0953-8984(97)74799-4

# Microstructural characterization of carbon films and $CN_x$ films produced by $N^+$ implantation

N Laidani†‡, A Miotello‡, A Glisenti§[+], C Bottani‖ and J Perriere¶

† Centro Materiali e Biofisica Medica, 38050 Povo, Trento, Italy

‡ Dipartimento di Fisica, Università di Trento, 38050 Povo, Trento, Italy

§ IBM Research Division, Almaden Research Center, San Jose, CA, 95120-6099, USA

‖ Istituto Nazionale per la Fisica della Materia, Dipartimento di Ingegneria Nucleare, Politecnico di Milano, via Ponzio, 34/3, 20133 Milano, Italy

¶ Groupe de Physique des Solides, CNRS, Université de Paris VII–VI, 2 place Jussieu, Tour 23, 75251 Paris, France

Received 23 May 1996, in final form 15 October 1996

**Abstract.** We report on a study of the electronic, chemical and lattice structure of carbon films and of the microstructural modifications induced by $N^+$ implantation. Correlations were made with the new mechanical properties of the implanted films. The C films were r.f. magnetron sputtered from a graphite target with Ar discharge. $N^+$ implantations were performed with energies ranging from 30 to 160 keV and at a fluence of $2 \times 10^{17}$ $N^+$ $cm^{-2}$. The effects of N on the structural and chemical properties of the C films were studied by means of x-ray photoelectron spectroscopy (XPS) and Raman scattering. Nuclear reaction analysis (NRA) and elastic recoil detection (ERD) were used to determine the atomic composition and density of the films. The carbon films consisted of two phases: microcrystalline graphitic domains dispersed in an amorphous matrix. The ratio of the hardness to the Young modulus, $H/E$, is comparable to that of diamond. $N^+$ implantation produces new bondings in these films, enhances the amorphicity and increases the disorder of the graphitic phase. The diamond-like features of the electronic valence band (strong s–p-orbital mixing) are preserved in the implanted films, together with the Young modulus of the network. Only the top of the valence band was affected by the ion irradiation. The new microstructure of the surface region of the implanted films resulted in an improved friction behaviour. $N^+$ implantation decreased the ratio $H/E$ to a value similar to that of metallic hard coatings.

## 1. Introduction

There is considerable interest in new materials like hard carbon films, with useful mechanical properties such as hardness, elasticity and low friction coefficient. A large number of film deposition methods have been employed to produce films with diamond-like properties. Recent investigations have been devoted to $CN_x$ compounds, the aim being to synthesize $\beta$-$C_3N_4$, a hypothetical compound whose bulk modulus should be at least as high as that of diamond. However, it has been found that $CN_x$ films with N/C atomic ratios lower than that of $\beta$-$C_3N_4$ still have interesting mechanical properties, being quite hard and elastic [1–3].

In order to synthesize carbon nitride films, many groups developed ion-beam-assisted deposition using energies typically in the range 5 eV–20 keV [4, 5]. $N^+$ implantation is

[+] Permanent address: Dipartimento di Chimica Inorganica Metallorganica ed Analitica, Università di Padova, via Loredan 4, 35131 Padova, Italy.

0953-8984/97/081743+19$19.50 © 1997 IOP Publishing Ltd

another possible technique for forming $CN_x$ layers. This technique looks promising as (i) it offers a more straightforward control of the nitrogen concentration and (ii) it is able to promote non-equilibrium phase formation. Covalent bondings between C and N induced by low-energy $N^+$ implantation (0.5–2 keV) in graphite have been studied by Gouzman *et al* [6] and, more recently, 100 keV $N^+$-implantation chemical effects in carbon films have been investigated by Xin *et al* [7].

In this work, we report on the $N^+$-implantation effects on the structural, compositional and chemical properties of a carbon network, the latter prepared by r.f. sputtering of a graphite target with Ar discharge. The effects of N on the film microstructure and chemistry were studied by means of x-ray photoelectron spectroscopy (XPS) and Raman scattering. Nuclear reaction analysis (NRA) was used to determine the atomic composition and the density of the films. The changes in the depth distribution of hydrogen induced by the $N^+$ implantation have been followed by elastic recoil detection (ERD). Hydrogen was not intentionally incorporated in the films—it came from gas-phase contamination.

The mechanical properties of the as-deposited and the implanted films have been studied in terms of Knoop microhardness and elastic modulus. The latter was deduced from the relative contraction of the diagonals of the Knoop indentations. Sliding friction measurements have also been performed.

## 2. Experimental details

### *2.1. Film growth and ion implantations*

The C films were sputter deposited, from a graphite target, on two types of substrate: silicon and cemented WC substrates. The use of the WC was necessary for samples subjected to mechanical measurements. The Si substrates were organically degreased in ultrasonic baths and then etched in hot $H_2SO_4$ and in dilute HF. The metallic substrates were mirror polished before the degreasing in ultrasonic baths was performed. The deposition was carried out in a r.f. planar magnetron discharge at a power of 100 W, in a 1 Pa argon atmosphere, and the substrates were kept at 573 K by means of external heating. The base pressure before deposition was less than $2 \times 10^{-5}$ Pa. The coatings were obtained at the floating potential. The target was sputter cleaned prior to each deposition, with a shutter shielding the substrate during this procedure.

After the deposition process, the film thickness was measured by means of a Dektak profilometer, with a typical error of 11%. Depending on the subsequent analysis of the samples, films of different thickness were produced:

(i) 100 nm film thicknesses were produced for ERD and NRA;
(ii) films of thickness ranging from 60 nm to 800 nm were prepared for XPS and Raman analyses; and
(iii) 900 nm films deposited on cemented WC were used for the mechanical and friction characterization.

The $N^+$ implantations in the C films were characterized for conditions of normal incidence, room temperature, a current density of about 5 $\mu$A cm$^{-2}$ and a fluence of $2 \times 10^{17}$ ions cm$^{-2}$. The choice of the ion energy was related to the film thickness in the following way:

(i) 30 keV for 60–100 nm films, the corresponding projected ion range, $R_p$, being 76 nm;
(ii) 90 keV for 400 nm films ($R_p = 210$ nm); and
(iii) 160 keV for 800–900 nm films ($R_p = 346$ nm).

The ion ranges, the concentration profiles of the implants, the sputtering losses and the nuclear energy losses were computed by means of the P-code program ('Ion Beam Profile Code', version 2.0, Copyright Implants Sciences Corporation, 1986–1987) and the TRIM'95 program [8].

The ion-implanted carbon films will be designated in the following as ii-$CN_x$.

### 2.2. Film characterization

The atomic composition of the films was determined by NRA and ERD. Absolute amounts of carbon, nitrogen and oxygen were obtained through the $^{12}C(d, p)^{13}C$, $^{14}N(d, p)^{15}N$ and $^{16}O(d, p)^{17}O$ reactions respectively. ERD was used to determine the absolute hydrogen content in the films. In this case, the samples were bombarded by 1.9 MeV $\alpha$-particles at an incidence angle of 15°, while the detection angle was set at 30°. The hydrogen concentrations have been extracted from the experimental data by the SENRAS simulation program [9].

XPS spectra were recorded in a Perkin–Elmer PHI 5600ci spectrometer with monochromatized Al K$\alpha$ (1486.6 eV) radiation; the instrument is equipped with a small-focus electron-extraction lens system, and an Ar-ion sputtering gun. The electron take-off angle was 45°. The working pressure was less than $2 \times 10^{-7}$ Pa. The spectrometer was calibrated by assuming the binding energy (BE) of the Au $4f_{7/2}$ line to be at 83.8 eV with respect to the Fermi level. Detailed scans were recorded for the C(1s), N(1s), Si(2p) and O(1s) regions. Sputter depth profiling was performed by rastering a 3 keV $Ar^+$-ion beam. The standard deviation in the BE values is 0.15 eV. After a Shirley-type background subtraction [10], the raw spectra were fitted using a non-linear least-squares fitting program adopting Gaussian–Lorentzian peak shapes for each peak [11]. The valence band spectra were deconvoluted using gaussian peak shapes. The atomic compositions were evaluated by using the Perkin–Elmer experimental sensitivity factors [12].

Room temperature Raman spectra of the films were recorded with a Jobin–Yvon T64000 spectroscope, using an $Ar^+$-ion laser as a light source operating at 514.5 nm.

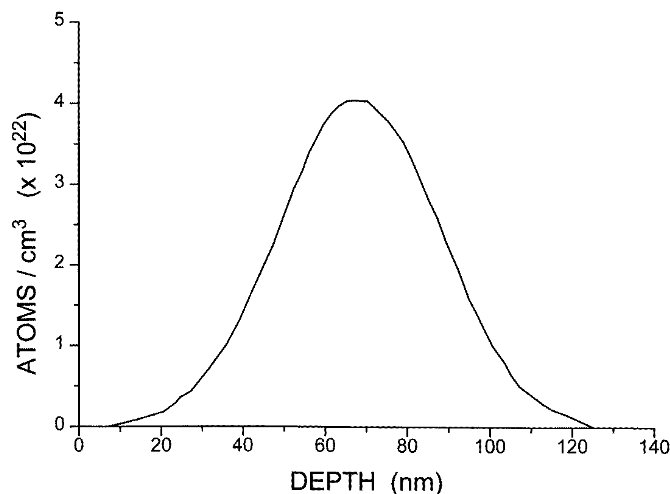


**Figure 1.** The calculated N depth profile in 30 keV, $2 \times 10^{17}$ atoms $cm^{-2}$ $N^+$-implanted carbon.

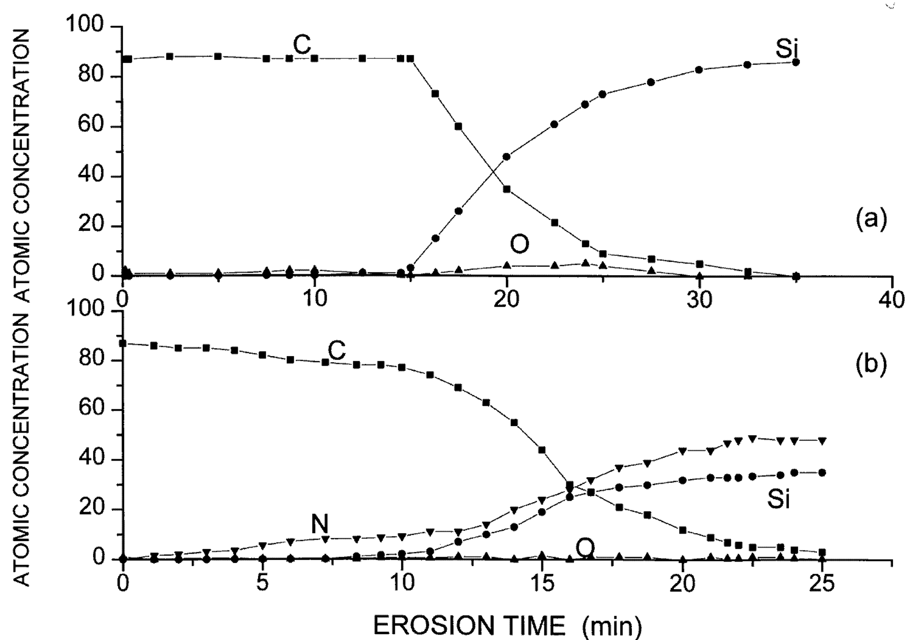


**Figure 2.** XPS concentration–depth profiles plotted as a function of erosion time: (a) in a 60 nm C film; and (b) in a 60 nm $N^+$-implanted C film (30 keV, $2 \times 10^{17}$ atoms $cm^{-2}$).

**Table 1.** The composition (atoms $cm^{-2}$) and density (g $cm^{-3}$) of the C and ii-$CN_x$ films.

| Sample | H ($\times 10^{15}$) (±5%) | O ($\times 10^{15}$) (±3%) | C ($\times 10^{15}$) (±10%) | N ($\times 10^{15}$) (±5%) | Density (±20%) | N/C (±15%) |
|---|---|---|---|---|---|---|
| C film | 205 | 40 | 824 | — | 1.73 | — |
| ii-$CN_x$ | 250 | 57 | 807 | 192 | 2.2 | 0.24 |

Knoop measurements were used to measure the film microhardness. Up to twenty indents were made at randomly chosen positions. The friction properties were evaluated using a scratch tester equipped with a 120° Rockwell C diamond indenter. The sample could be moved across the diamond tip while the normal load was maintained constant. The measurements were made in air. Two calibrated sensors served to measure the normal and the tangential forces. The samples were degreased before the friction measurements were made.

## 3. Results

### *3.1. The atomic composition and density of the C films and the ii-$CN_x$ films*

The experimental results on atomic composition obtained with NRA and ERD for unimplanted and $N^+$-implanted films are presented in table 1. Both films were 100 nm thick and the implantation energy was 30 keV. With such an energy, the implanted layer would extend from ~15 nm to ~120 nm in depth, as shown in figure 1 which represents

the predicted depth distribution of the implants. Thus, 100 nm films are expected to retain the major part of the implanted atoms.

Depth–concentration profiles of the elements of a 60 nm C film deposited on silicon, as obtained by XPS, are given in figure 2(a). The C films contain small amounts of oxygen on the film surface and in the bulk. However, it is mostly concentrated at the film/substrate interface, due to the native silicon oxide present on the substrates before deposition.

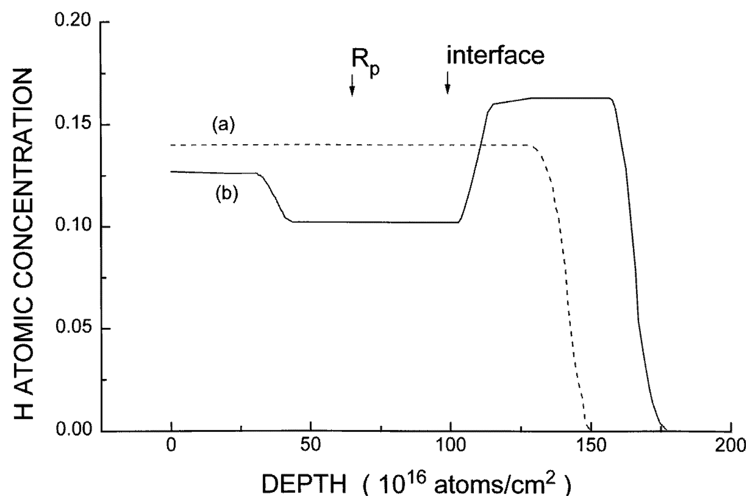


**Figure 3.** In-depth H profiles in C films (a) before and (b) after $N^+$ implantation.

Although it was not intentionally added, the samples contained hydrogen, in higher quantity than oxygen (H/C atomic ratio = 0.25 and 0.31 for the C films and the ii-$CN_x$ films respectively). However, the values reported in table 1 include the H content both in the film and in the substrate. The actual amount of H in the film is found to be somewhat lower as it is shown in figure 3. In this figure the ERD concentration profiles of hydrogen, as a function of depth, in C and ii-$CN_x$ films (profiles (a) and (b), respectively) are reported. The film/substrate interface position (marked in the figure) has been assigned on the basis of the NRA results of the films. In the unimplanted specimen, the hydrogen profile is flat and extends down into the substrate. The actual H/C ratio in the C films is 0.14.

Hydrogen very probably diffused from the plasma phase into the film and into the substrate, in the course of the deposition process. The diffusion into the substrate probably occurred during the target pre-sputtering sequence. The duration of the latter was varied from 15 min to 40 min. So, the hydrogen content in the substrate is expected to vary from one sample to another. On the other hand, the results of ERD analysis of the graphite target did not reveal hydrogen, from which we conclude that the presence of H in the Ar plasma originated from gas-phase contaminants such as water vapour.

The density (in g cm$^{-3}$) of the C and ii-$CN_x$ films, as deduced from the NRA and ERD results and the geometrical thicknesses, are also given in table 1. The density value of the C film, estimated as $1.73 \pm 0.34$ g cm$^{-3}$, is less than that of graphite (2.09–2.23 g cm$^{-3}$) and that of diamond (3.50–3.53 g cm$^{-3}$) [13]. It is rather typical of amorphous films [14, 15].

For the ii-$CN_x$ films, the NRA results show that the retained N dose value in the films was equal, within the detection error limits, to the incident dose and yielded a global N/C

atomic ratio of 0.24.

The atomic density of the C films was increased by $N^+$ implantation. The NRA results did not show a significant change of the areal density of the C atoms after $N^+$ implantation. In fact, the P-code calculations give a sputtering loss of only 8% of the film thickness, a value less than the NRA error limit for carbon detection. So, the same thickness as that of the unimplanted film (100 nm) has been used to calculate the density of the ii-$CN_x$ films. The value is given in table 1.

**Table 2.** The Knoop microhardness $H$, index of rigidity $H/E$, Young modulus $E$ and friction coefficient $\mu$ of the C and ii-$CN_x$ films. For comparison $H$- and $E$-values of diamond are also reported as well as the Knoop microhardness of the cemented WC substrates.

| Material | $H$ (GPa) | $H/E$ | $E$ (GPa) | $\mu$ |
|---|---|---|---|---|
| C film | $36.7 \pm 3.7$ | 0.08 | 471 | $0.20 \pm 0.02$ |
| ii-$CN_x$ | $15.4 \pm 2.0$ | 0.03 | 441 | $0.06 \pm 0.01$ |
| WC substrates | $27.3 \pm 3.0$ | — | — | — |
| Diamond [17, 19] | 100–103 | 0.09–0.10 | 1050 | — |

Implantation with 30 keV ions resulted in a changed hydrogen distribution, as seen in figure 3, profile (b). The ii-$CN_x$ film exhibits a marked H depletion in a broad region around the ion projected range (marked in the figure). The features of the hydrogen profile in the ii-$CN_x$ film, are similar to what is reported in the literature for alloys under ion bombardment and attributed to a radiation-enhanced interstitial mechanism of transport [16]. Although the global H amount, as reported in table 1, was in this case higher than in the unimplanted sample (this was probably due to different substrate contamination levels as discussed above), the implanted film itself had less hydrogen than the unimplanted film.

### *3.2. Mechanical characterization of the C films and ii-$CN_x$ films*

The mechanical performances of the C and nitrogen-containing C films as regards hardness, elastic modulus and friction are key features for their technological use. In table 2 we report the values of the Knoop microhardness ($H$) of the C and ii-$CN_x$ films obtained by 160 keV $N^+$ implantation together with the Young modulus $E$, the ratio $H/E$ and the friction coefficient.

We chose hard cemented WC substrates to make sure that the measured hardness values are related to the films, 900 nm thick, and not strongly influenced by the substrate. A load of 0.25 N was used for the C samples. The penetration depth of the indent (~1/30 of the long diagonal) is calculated as 330 nm. A lower load, 0.15 N, was applied to the ii-$CN_x$ films to achieve comparable penetration depth (380 nm) and projected ion range (346 nm) values. Besides this, the measured hardness values of the unimplanted and implanted films can be directly compared since the corresponding indentation depths are somewhat similar.

The C films are seen to be quite hard and belong to the diamond-like carbon class of materials [17]. For comparison, the Knoop microhardness value obtained for the cemented WC substrate under a 0.25 N load and the microhardness of diamond, as reported in literature, are also given in table 2.

The introduction of N in the C films results in a hardness reduction. This decrease in microhardness observed in the N-containing C films can be understood in terms of the new chemical bonds established between C and N, as we will see in section 3.4, but the expected structural damage introduced with N ions in the ii-$CN_x$ films is very probably

an additional factor of the film softening. For 160 keV ion energy, the nuclear energy loss amounts to 43 eV nm$^{-1}$. In fact, the bombardment-induced defects can lead to an increased defect concentration. However, a comparison of this hardness value with those of some representative hard materials such as transition metal nitrides [18] allows one to conclude that the ii-CN$_x$ films can still be considered quite hard, and this is a technologically important aspect.

Although the C-film hardness was to some extent sacrificed by N$^+$ implantation, interestingly the elastic properties of the films were not affected. One way to measure the Young modulus of a material is to observe the relative contraction of the surface diagonals of the Knoop indentations [19]. This method enables one to determine the ratio of the hardness to the elasticity modulus, $H/E$, from which $E$ can be derived. The ratio $H/E$, also named the rigidity index of the material, is determined as follows:

$$b'/a' = b/a - \alpha H/E \quad (1)$$

where $b/a = 1/7.11$ is the nominal ratio of the short to the long half-diagonal, $b'/a'$ is the corresponding ratio after recovery, and $\alpha$ is an empirical dimensionless constant ($\alpha \approx 0.45$).

Before applying equation (1) to determine the ratio $H/E$ for the experimental films, we tested it with materials having known values of $H$ and $E$. To this end we tested crystalline $ZrO_2$ and $Al_2O_3$ (sapphire) and we used the nominal values of $H$ and $E$ from [18]. The experimental values obtained with the method described above and the nominal values of $H/E$ are found to agree within an experimental error of 13%.

The $E$-values for C and ii-CN$_x$ are reported in table 2 as well as the ratios $H/E$ from which they were deduced. The C films exhibit a high value of $H/E$, comparable to that of diamond [18, 20]. In ii-CN$_x$ films, the ratio $H/E$ dropped to less than half the value of the C films. It is known that the tendency of a material to fracture scales with the value of $H/E$ [21]. In this framework, while the C films are obtained with a value of $H/E$ similar to that of covalent hard materials, the ii-CN$_x$ films behave like metallic hard materials such as the transition metal nitrides (e.g. TiN, CrN or ZrN for which the values of $H/E$ are also near 0.03 [18]).

As can be seen in table 2, the Young modulus of the C films does not significantly change after N$^+$ implantation. This is an important result since the elasto-plastic properties of a coating are of great importance for its adhesion performance and its wear behaviour.

Also of particular interest in view of technological applications is the friction coefficient of the C-based films. The same samples used for the hardness measurements were also used for friction measurements. The friction coefficient values ($\mu$) of C and ii-CN$_x$ films are given in table 2. We reported the mean values of $\mu$ obtained for a load range of 1 to 12 N. In this load range, the films were still adhering to the cemented WC substrates, as we observed by optical microscopy. N$^+$ bombardment had an important effect on the friction behaviour as $\mu$ dropped to a third of its initial value.

### *3.3. Electronic structure of the C and CN$_x$ films*

#### *3.3.1. The C films*

(i) *X-ray-excited Auger spectra.* In figure 4, the C KVV Auger derivative spectrum recorded on a C-film surface is reported (spectrum (a)) along with that of diamond (b) and graphite (c) adapted from [22]. The Auger spectrum of diamond contains four peaks (labelled A, A′, B and C). The peak A′ is less intense than the main peak A and the peaks B and C have been ascribed to surface and bulk plasmon loss peaks respectively. The spectrum of graphite consists of three peaks (labelled A, A′ and B). The peak A arises as

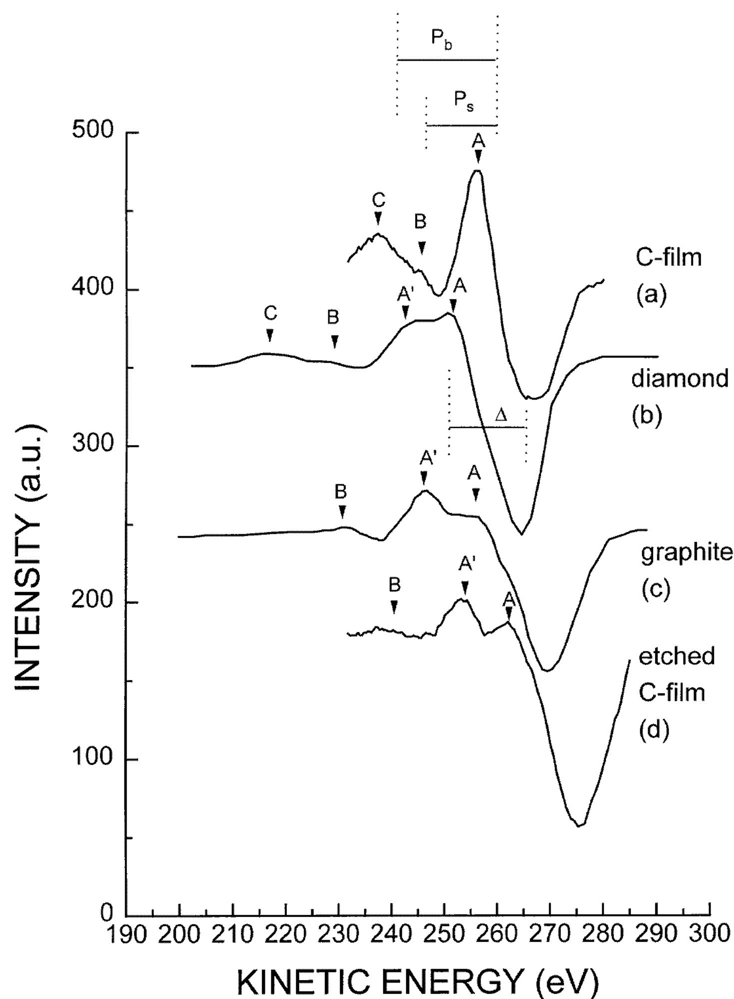


**Figure 4.** C KVV x-ray excited Auger spectra from: (a) a C-film surface; (b) diamond, adapted from [22]; (c) graphite, adapted from [22]; and (d) a C film after $Ar^+$ etching.

a wide shoulder of peak A′ (the main peak here) and peak B is relative to surface plasmon loss. No bulk plasmon loss occurs in the Auger spectrum of graphite.

Let us compare the features of the experimental C-film spectrum to those of diamond and graphite spectra, disregarding the energy shifts of the spectra relative to one another. Such energy shifts were very probably due to sample charging during the analysis. The features of the experimental spectrum of the C film (a) are labelled in the same manner as those of (b) and (c). Although narrower, the C-film spectrum grossly resembles much more that of diamond than that of graphite. In particular, the presence of the two plasmon loss peaks and the absence of the broad shoulder A as in spectrum (c), the fingerprint of a graphitic structure, rather indicate a diamond-like character of the C films, in agreement with their mechanical properties.

However, the differences between the C film and diamond reflect some differences in the structure and the chemical environment of the C atoms in these two materials, as listed below.

(1) From the standpoint of a fingerprint, the Auger derivative spectrum of diamond is characterized by a peak-to-peak width (labelled $\Delta$ in spectrum (b)) of the main transition of 13 eV [22], while in graphite this width is of 23 eV. In the C-film spectrum, the width of the major peak is $\sim$11 eV, a value slightly less than that of diamond and far from that of graphite. Although we do not have a totally satisfactory explanation for such a narrowing of the major peak (with respect to diamond), a trivial one would be that it is an effect of the surface contamination. It is generally observed in metals, in the Auger analysis, that chemisorbed layers may affect the features of the Auger transition pertinent to the substrate elements [23, 27]. Note that oxygen has always been detected on the surface of the film. The narrowing of the main peak may be due as well to a specific microstructure of the film.

(2) The fine structure A′, on the low-energy side of the main transition, is not resolved in the C-film spectrum. Bearing in mind that the electronic properties of a solid are determined by short-range order [24], an amorphous state and a crystalline state reproduce the same gross spectral features, differing only in the fine spectral features. The absence of peak A′ points towards the absence of a long-range order of the carbon network. It must be noted that films presenting an x-ray-excited C KVV Auger spectrum similar to the one that we obtained have been analysed by electron diffraction and found to be totally amorphous [25].

(3) The positions of the two plasmon peaks B and C for the C film are nearer to the main peak A. The surface and the bulk plasmon loss energies (indicated as $P_s$ and $P_b$ respectively in spectrum (a)), which are the differences between the energies of the maxima in the integral spectrum, are 13 eV and 19.4 eV for the C film. In diamond the plasmon loss peaks occur at 28 and 38 eV away from the main transition [22]. Since the plasmon loss energy is proportional to the atomic density through the electron density, it is clear from the comparison of these values with that the C film that the latter is much less dense than diamond. Further, the atomic density of the C film has been deduced from the bulk plasmon loss peak energy and compared to the value obtained with NRA. The energy of the plasmon oscillation of the valence electrons is given by $E = h\omega_p/2\pi$ where $\omega_p$ is the bulk plasmon frequency. It depends on the electron density, $n$, as

$$\omega_p = (4ne^2\pi/\epsilon m^*)^{1/2} \tag{2}$$

where $e$ and $m^*$ are the electron charge and the electron effective mass [26]. The latter has been taken equal to the free-electron mass.

Assuming four valence electrons per atom, the electron density ($n$) yields a mass density value of $1.70 \pm 0.16$ g cm$^{-3}$ for the C film, a value in good agreement with that obtained with NRA (table 1).

The spectrum (d) of figure 4 is the C KVV spectrum obtained from a C film after an $Ar^+$ erosion in the analysis apparatus. The strong similarity of its lineshape with that of graphite indicates a strong change of the film structure towards a graphitic one. The graphitization of the carbon network is also supported by the energy shift of the spectrum to higher kinetic energies with respect to that of the unetched film (spectrum (a)), proof of an increased electrical conductivity. Due to this behaviour, the electronic structure investigations were limited to the surface layers of the films.

(ii) *XPS valence band spectra.* The valence band (VB) structure of the surface layers of C films is shown in figure 5 (spectrum (a)). The energy scale was established with respect to the Fermi level, $E_F$ (the zero-energy point). The spectrum is dominated by two

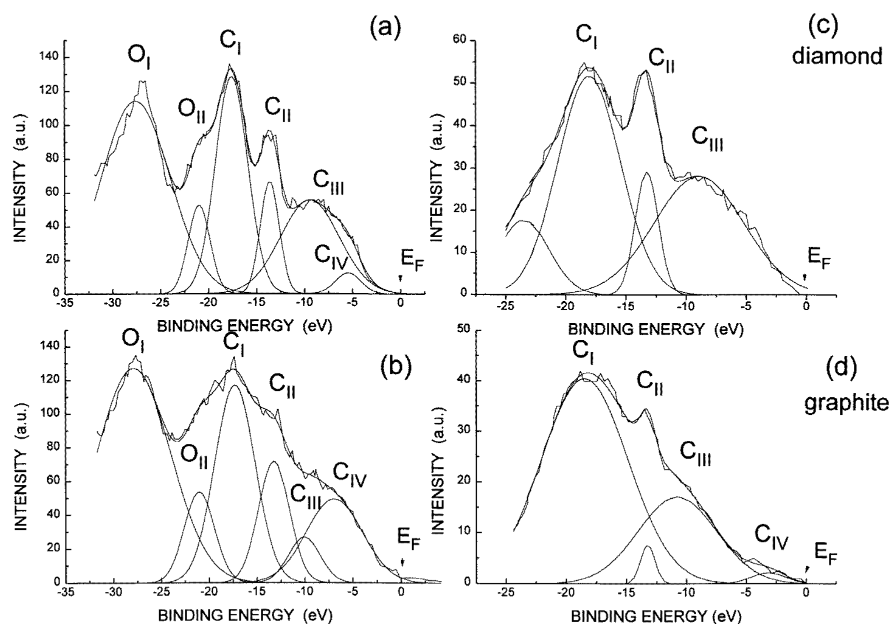


**Figure 5.** XPS valence band spectra from (a) a C film, (b) a ii-$CN_x$ film, (c) diamond, adapted from [29], and (d) graphite, adapted from [29].

prominent peaks at about −26 eV and −17.5 eV, labelled $O_I$ and $C_I$ respectively. Two other minor peaks, at about −13 eV and −9 eV, are also present. The $O_I$ peak is attributed to the oxygen 2s electronic core level [25, 26]. Oxygen contamination accounts also for the shoulder, $O_{II}$, to the left of peak $C_I$ [28].

Restricting consideration to the energy range 0–20 eV, the two sharp maxima at −17.5 eV ($C_I$), −13 eV (labelled $C_{II}$) and the broader third one, lying at around −9 eV (labelled $C_{III}$), agree well with the VB structure of diamond, as reported in the literature [29, 30]. In addition, the top of the VB tails off sharply in the experimental spectrum of the C film, as in diamond, while in graphite it tails off slowly towards low binding energies. The VB spectra of diamond and graphite, adapted from [29], are shown in figures 5(c) and 5(d) respectively.

A theoretical framework exists for diamond and graphite [31, 32], from which it is possible to extract some information about the electronic structure of the C films. We fitted the diamond VB spectrum to three gaussians, $C_I, C_{II}$ and $C_{III}$, in the energy range 0 to ∼−20 eV (spectrum (c)). A fourth peak on the lowest-energy side of the spectrum has been added to simulate the artificial tail of this spectrum in this energy range [29]. Peak $C_I$ corresponds to an s-like occupied valence band, while the peak $C_{III}$ accommodates p–$\sigma$ electronic levels which drop off very sharply towards $E_F$. A mixture of s and p electronic levels gives rise to peak $C_{II}$ in the VB spectrum. We deconvoluted the VB spectrum of graphite with four peaks. In graphite, the first three peaks, $C_I, C_{II}$ and $C_{III}$, correspond to the $\sigma$-band (s–$\sigma$, sp–$\sigma$ and p–$\sigma$), as in diamond, while the fourth peak $C_{IV}$, tailing towards $E_F$, is related to the p–$\pi$ band.

In graphite, the $2p_z$ atomic orbitals are, to a large extent, unmixed with the other bands and since the XPS cross-section of the s-like states is higher than that of the p states [29],

this results in a strong predominance of the peak $C_I$ merging from purer s states in the VB spectrum with respect to diamond. Thus, in graphite, the peak $C_I$ dominates the VB spectrum more than in diamond and the peak $C_{II}$ is considerably attenuated, as can be seen in spectrum (d). As the differences between the VB spectra of diamond and graphite are due essentially to different s–p mixing extents ($sp^3$ versus $sp^2$), which is reflected in their different bonding configurations (totally isotropic in diamond and anisotropic in graphite), the relative contributions of the peaks $C_I$, $C_{II}$ and $C_{III}$ to the total spectrum of a C film can provide a way to characterize its bonds.

In this respect, the VB spectra of the C film was resolved into four peaks in the 0 to $\sim -20$ eV range. As the experimental spectrum has not been corrected for inelastic losses, an artificial tail persists at the bottom of the VB and makes difficult a perfect fitting of the spectrum in this region, as can be seen for the $O_I$ peak in figure 5(a). Nevertheless, the remaining portion of the spectrum, which is of greatest interest for this study, can be optimally fitted.

**Table 3.** Individual peak widths and relative weights of the carbon VB spectra of C and ii-$CN_x$ films. For comparison, the relative weights of the individual peaks of diamond and graphite spectra are also given.

| | Peak width (eV) | | | |
|---|---|---|---|---|
| | $C_I$ | $C_{II}$ | $C_{III}$ | $C_{IV}$ |
| C film | 3.3 | 1.9 | 6.1 | 2.5 |
| ii-$CN_x$ | 4.3 | 3.2 | 3.6 | 5.6 |
| | Peak relative weight | | | |
| | $C_I$ | $C_{II}$ | $C_{III}$ | $C_{IV}$ |
| C film | 0.45 | 0.14 | 0.36 | 0.03 |
| ii-$CN_x$ | 0.44 | 0.15 | 0.08 | 0.20 |
| Diamond | 0.50 | 0.10 | 0.4 | — |
| Graphite | 0.70 | 0.02 | 0.30 | 0.01 |

A comparison of the deconvoluted experimental spectrum of the C film with the diamond and graphite spectra lets one conclude that there is a similarity of the VB spectrum of the C film with that of diamond, in the energy range corresponding to the $\sigma$-band. In table 3 we give the peak width and the relative weight of each of $C_I$, $C_{II}$, $C_{III}$ and $C_{IV}$ for C and ii-$CN_x$ films, diamond and graphite, as obtained from curve fitting. The relative contribution of a peak is here defined as the ratio of its area to the total area of all C peaks. It can be seen that the relative weight of peaks $C_I$ and $C_{II}$ in the C film is much closer to that in diamond than that in graphite. This result suggests that that in the C film, the C atoms are bonded mainly in a three-dimensional array, as in diamond, and not in planar sheets as in graphite.

The energy positions of the three peaks of the $\sigma$-band are approximately identical for diamond, graphite and C film and cannot serve as a basis for comparison. However, in contrast to the case for diamond, the top of the VB spectrum of the C film, in addition to the p–$\sigma$ peak at $\sim -9$ eV ($C_{III}$), consists of another small peak (labelled $C_{IV}$) located at $-5.5$ eV. The presence of such a peak is attributed to p–$\pi$ electronic states, by analogy with graphite, i.e. to a significant number of threefold-coordinated carbon atoms. However, this peak arose at an energy significantly higher than that of the p–$\pi$ band in graphite ($-2.8$ eV). This result is a further indication that the $sp^2$ sites in the C film were bonded differently to in graphite. Besides this, note the sharp cut-off of the top of the VB—a situation quite

different to that for graphite.

As discussed in the previous section, the lineshape of the C KVV Auger transition suggested an essentially amorphous structure of the C films. On the other hand, the features of the C KVV Auger spectrum (figure 4) are related to the density of valence states [31, 33], as are those of the VB spectra (figure 5). Consequently, we expect that the characteristics of the VB spectrum obtained by XPS are essentially those of an amorphous phase. It follows that a structural model for these C films should account for a highly connected amorphous network (as indicated by the strong $C_{II}$ peak), composed of both $sp^3$- and $sp^2$-hybridized atoms. In addition, the high value of the ratio $H/E$ (table 2), close to that of diamond, is a further indication of a high connectivity of the covalent carbon network [20].

In the following section, we will examine the effects of the $N^+$ implantation on the particular structure of these C films.

*3.3.2. The XPS valence band spectrum of an $N^+$-implanted film.* The VB spectrum of the carbon film surface after $N^+$ implantation is shown in figure 5(b). The film was 60 nm thick and implanted with 30 keV ions. The oxygen peak at $\sim -26$ eV is still present. The remaining part of the spectrum has lost its fine structure. To better evaluate the effects of $N^+$ implantation on the electronic structure of the films, the ii-$CN_x$ VB spectrum has been deconvoluted into six peaks, two of which pertain to oxygen in the $-20$ to $\sim -30$ eV range as indicated earlier. Although the VB spectrum in the energy range 0 to $\sim -20$ eV is still fitted by four peaks, as in the C-film spectrum, appreciable differences exist between the two spectra. One effect of the $N^+$ implantation was the broadening of the peaks $C_I$ and $C_{II}$, related probably to an increased disorder, due to an increased defect density. However, the relative contribution of these two peaks to the whole carbon spectrum remained unchanged, as shown in table 3.

Thus, although significantly broadened, the bottom of the carbon valence band (peaks $C_I$ and $C_{II}$) still resembles that of the unimplanted carbon with regard to the s–p-state mixing. This means that most of the C atoms were still isotropically bonded. This is in good agreement with the modulus of elasticity of the C films, which remained unchanged after $N^+$ implantation (table 2).

In contrast, the p band (p–$\sigma$ and p–$\pi$ subbands) underwent great modifications on $N^+$ bombardment. First of all, the relative weights of the p–$\sigma$ ($C_{III}$) and p–$\pi$ ($C_{IV}$) bands are inverted (table 3). It is important to note that no N signal has been detected on the surface of the film, as can be understood from the N concentration profile given in figure 2(b) along with those of C, O and Si in ii-$CN_x$ film. (The modifications affecting the film/substrate interface region will not be discussed here, being beyond the scope of this work.) The theoretical N depth distribution also excludes its presence at the surface of the film (see figure 1). So, the increased contribution of peak $C_{IV}$ in the VB spectra after $N^+$ implantation cannot be attributed to new states pertaining to N. The observed modifications are thought to be caused only by the structural damage created by the ion bombardment.

Another change brought about by the implantation concerns the widths of the peaks $C_{III}$ and $C_{IV}$. As shown in table 3, peak $C_{III}$ becomes narrower after bombardment, while peak $C_{IV}$ is much wider. It is also interesting to note that the $N^+$ implantation altered the p–$\pi$-band width (5.6 eV after implantation versus 2.5 eV before) while it did not alter significantly the total $\sigma$-band width (11.1 eV after versus 11.3 eV before). The total $\sigma$-band width is taken as the sum of the $C_I$, $C_{II}$ and $C_{III}$ peak widths. The $\pi$-states appear to be more affected by the structural damage accompanying the ion bombardment than the whole $\sigma$-band.

*3.4. $N^+$-implantation-induced chemical modifications*

The chemical modifications introduced by 30 keV $N^+$ implantation in a 60 nm thick C film have also been studied by XPS analysis. The VB and the C KVV Auger transition analysis results exposed in the above sections concerned only the surface region of the films. To investigate the chemical fate of the implanted nitrogen, the ii-$CN_x$ film has been etched with Ar ions in the XPS apparatus.

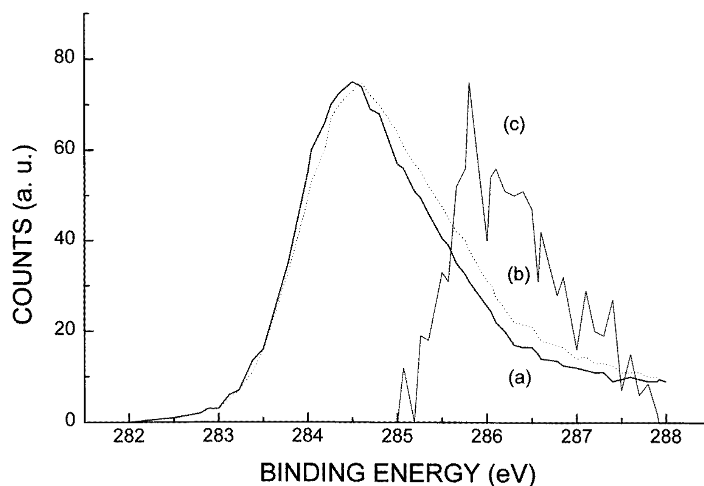


**Figure 6.** XPS spectra of C 1s recorded after 3 min of etching time in (a) a C film and (b) a ii-$CN_x$ film, and (c) the difference spectrum.

The creation of new chemical bonds in the C films following $N^+$ implantation has been studied by comparing two C 1s spectra shown in figure 6. In this figure, spectrum (a) has been recorded for the unimplanted film and spectrum (b) corresponds to the implanted film, after 3 min of etching time The difference curve (c) shows the presence of a new contribution centred at around 286 eV. This binding energy is consistent with that of C 1s in CN bondings [34].

Figure 7(a) shows the curve fitting of the C 1s spectrum, recorded for ii-$CN_x$ film after 6 min of etching time. The peak is asymmetrical with a maximum at 284.4 eV and a significant high-binding-energy tail. Peak synthesis gives individual peaks at approximately 284.4 eV, 285.4 eV and 286.4 eV. We assign the two first peaks (labelled '1' and '2' in figure 7(a)) respectively to C–C bondings in aromatic rings as in graphite and groups involving only C or C bound to H in non-aromatics [23]. In the latter case, C bound to itself and/or to hydrogen only, no matter what the hybridization, should give C 1s at ∼285 eV. More generally, this contribution to the C 1s spectrum is attributed to amorphous carbon [35, 36].

The atomic ratio between the graphitic carbon (C 1s at ∼284.4 eV) and the amorphous carbon (C 1s at ∼285.4 eV) is about 3.5 and does not significantly change through the film depth. Such a value would mean that the films were essentially graphitic, in contradiction with the x-ray Auger results and the VB characteristics. However, this ratio value is thought to be far from the actual one. It probably derives from the graphitization caused by the Ar-ion etching used for the profiling (see figure 4, spectrum (d)).

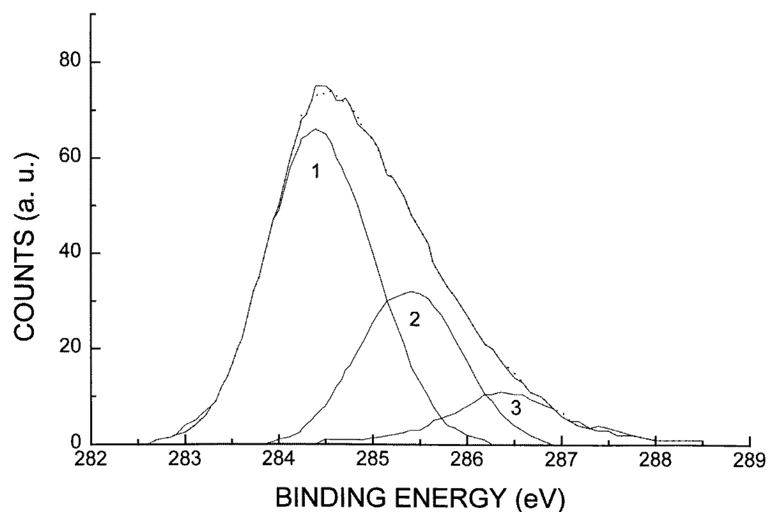


(a)

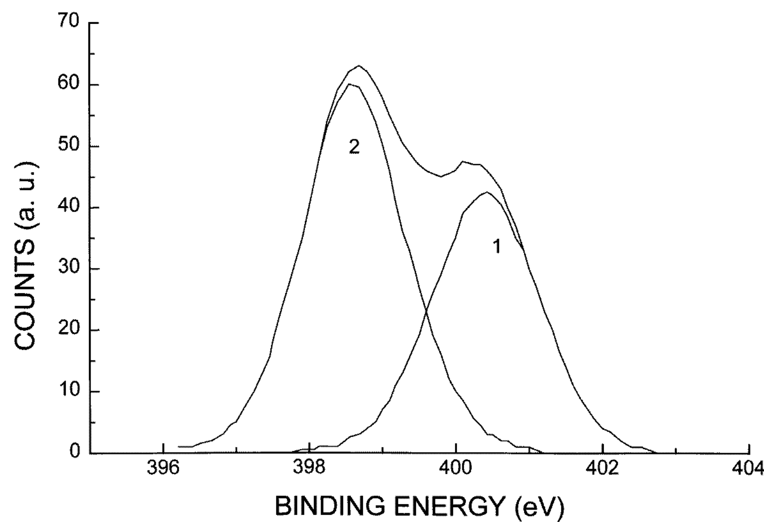


(b)

**Figure 7.** (a) The deconvoluted C 1s spectrum from an ii-$CN_x$ film. (b) The deconvoluted N 1s spectrum from an ii-$CN_x$ film.

Figure 7(b) shows the N 1s band of the XPS spectra, which appears as a doubly peaked spectrum. Curve fitting gives two peaks at 398.6 eV and 400.4 eV approximately, with a mean relative ratio of 1.2, without significant changes through the film depth. The two N 1s peaks have been observed by many authors in nitrogen-containing films produced by various processes, and are taken to indicate that, in the ii-$CN_x$ films, the implanted N bonded covalently to C. As for the chemical states of the implanted N atoms, many nitrogen-containing groups give N 1s binding energies in the narrow range 399–401 eV

in which the high binding energy of the experimental N 1s spectrum (labelled '1') arises. Published XPS data [37, 38] indicate that this peak may include C and N bondings as in Ph–$NH_2$, PhC≡N, Ph–N=N–Ph (where Ph stands for an aromatic nucleus) and also in linear >C=N–. According to Boyd *et al* [4], it is due to N–$sp^2$ C bondings as in >C=N–, in agreement with the conclusions of Ricci *et al* [39] who compared XPS and infra-red absorption results. In turn, most workers agree on attribution of the peak in the region 398.4–398.6 eV (labelled '2') to the nitrile (–C≡N) group [37–39]

The N/C atomic ratio at which carbon and nitrogen participate in the new CN bondings varies through the depth. It follows the N concentration. It increases from 0.6 when N amounts for 5 at.%, to reach 1.8 when N is present at 20 at.% in the film depth.

### *3.5. N effects on the lattice structure of the carbon films*

Raman spectroscopy is a common tool for the characterization of the structure of C-based materials and it is useful for the study of disorder and crystalline structures in carbon films. The Raman spectra of both diamond and graphite show well-known crystalline structures of carbon [40]. Polycrystalline graphite exhibits in its first-order Raman spectrum two lines: one at about 1580 $cm^{-1}$ called the G line, and another line at 1355 $cm^{-1}$, called the D line. The latter is known to appear in the Raman spectrum of microcrystalline graphite with a cluster size less than 25 nm. The two lines mentioned are in practice the lines most used to characterize carbon-based materials.

The Raman analysis of our carbon films has been mainly used (1) to check the composite properties of the films and (2) to investigate the different degree of disorder of the films. It is known that bond-angle disorder [30] or bridging in graphite [41] can modify the spectral properties, including a downshift in frequency or a broadening of the G and D peaks. In this work, it constitutes a useful complementary technique to XPS analysis since, with the latter, the analysis of the electronic states of carbon is limited to the surface layers.

Figures 8(a) and 8(b) compare the Raman spectra of a C film (a) and an ii-$CN_x$ film implanted with 90 keV $N^+$ ions (b). The difference in intensity of the two spectra is related to the difference in thickness of the films: 800 nm and 400 nm for the C film and the ii-$CN_x$ film respectively. The Raman spectrum of the C film consists of a twin-peaked band (figure 8(a)). The peaks, which are broad and of almost equal intensity, develop at about 1360 $cm^{-1}$ and 1590 $cm^{-1}$.

The two lines further broaden and coalesce into a featureless spectrum extending from ~1100 $cm^{-1}$ to ~1800 $cm^{-1}$ when the carbon film is implanted with nitrogen, as can be seen in figure 8(b). The additional very sharp line, at ~1554 $cm^{-1}$, which appears in each spectrum, pertains to oxygen.

Through a fitting procedure applied to the experimental spectra, more insight into the microstructure of these films can be gained. Each of the two spectra was deconvoluted into three broad peaks centred at 1360 $cm^{-1}$ (peak D), 1500 $cm^{-1}$ (peak A) and 1590 $cm^{-1}$ (peak G). According to the results reported in the literature regarding diamond and graphite, we assign the low-frequency band (D) to phonons associated with disordered microcrystalline graphitic domains. The peak at 1500 $cm^{-1}$ (A) is attributed to C–C vibration in an amorphous network, composed of an atomically mixed structure of threefold- and fourfold-coordinated carbon [42–44]. The presence of this feature would be in good agreement with the valence band characteristics of the C and ii-$CN_x$ films.

From these results, we conclude that the C films are of composite nature as they consist of two phases: microcrystalline graphite dispersed in an amorphous phase, the latter formed by $sp^2$ and $sp^3$ sites. The graphite content in this composite structure should amount to

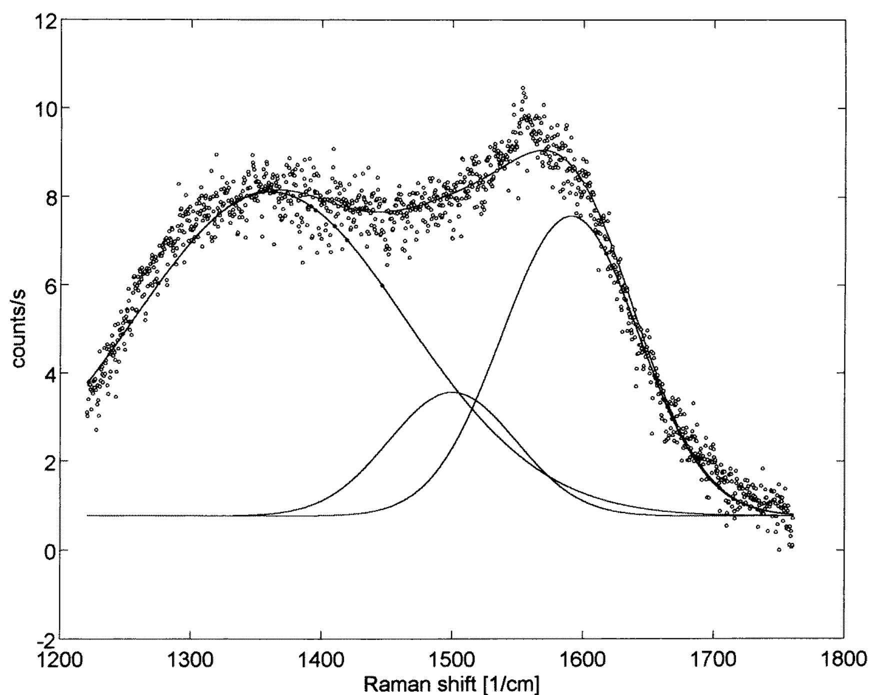


(a)

**Figure 8.** Raman spectra of (a) C film and (b) ii-$CN_x$ film.

**Table 4.** Raman individual peak widths for C and ii-$CN_x$ films and the area ratio A/G of the amorphous phase (A) and the graphite (G) peaks.

| Films: | C film | | | ii-$CN_x$ Film | | |
|---|---|---|---|---|---|---|
| Peaks ($cm^{-1}$): | D (1360) | A (1500) | G (1590) | D (1360) | A (1500) | G (1590) |
| Width ($cm^{-1}$): | 104 | 49 | 52 | 128 | 73 | 57 |
| A/G: | | 0.38 | | | 0.80 | |

only a small fraction, as the low-density value of the films and the XPS results indicate. The strong graphite Raman signal is due to its high absolute scattering cross-section with respect to those of other forms of carbon [40].

Table 4 gives the three gaussian widths used in the peak synthesis, along with the area ratio of the amorphous phase and the graphite peaks, A/G, for the unimplanted and implanted films. It emerges that $N^+$ bombardment of the film had as its main effect in significantly increasing the amorphicity of the network as is evident from the increased value of the ratio A/G for the ii-$CN_x$ film spectrum. Besides this, the structure of the remaining graphitic domains is affected also by the irradiation. The G and, to a much greater extent, the D peak become broader in the ii-$CN_x$ film spectrum than in the corresponding C film, indicating an increase of the structural disorder. It is known that the D line is more sensitive to disorder than the G line [45]. Like for the graphitic domains, the amorphous phase structure is also

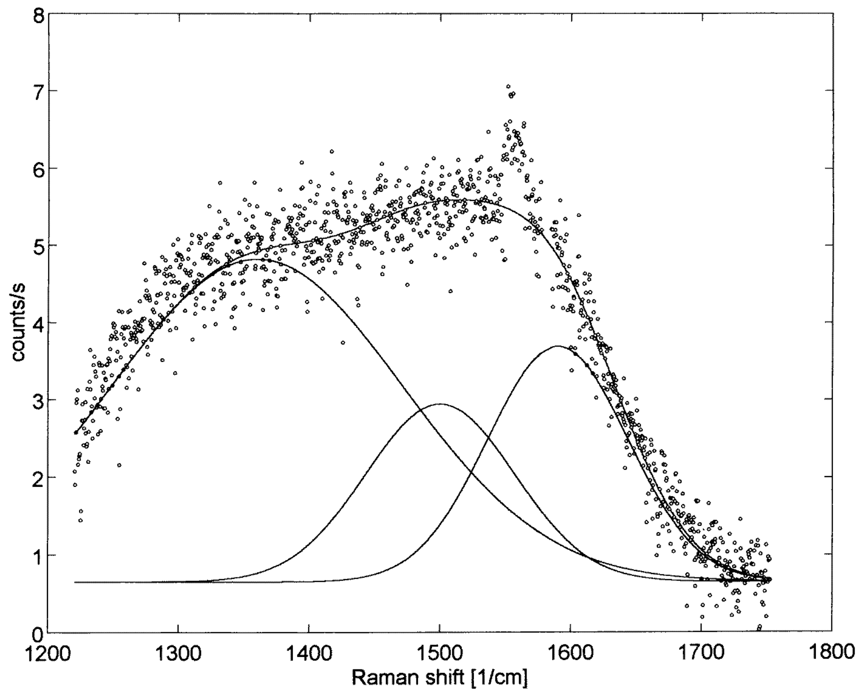


(b)

**Figure 8.** (Continued)

affected by the $N^+$ implantation, as shown by the strongly increased width of the peak A (table 4), probably due to an increase of defect concentration, in agreement with the VB features and the observed film softening.

## 4. Discussion

We have found that the atomic density of a C film, as deduced from the bulk plasmon loss energy in the C KVV Auger spectrum, matches, within the error limits, the value obtained from the NRA measurements. This finding indicates that the x-ray Auger analysis gives the major intrinsic features of the films, and among them the extent of DLC character, a result which is also supported by the valence band spectrum and by the mechanical properties of the films (high hardness and elasticity). The present results do not allow us to reach a conclusion as to the $sp^3/sp^2$ ratio; nevertheless they do give elements of a structure model.

Although Raman results indicate a composite microstructure of the C films (microcrystalline graphitic domains coexisting with an amorphous phase), the C KVV spectrum is consistent with a dominant amorphous structure, a $sp^3$–$sp^2$-site mixture bonded in a highly connected network, as revealed by the VB spectrum.

In the $N^+$-implanted films, N is covalently bonded to C. The XPS results show that the $>$C=N group and the peripheric group–C≡N are good candidates for describing the new chemical bonds. These new bonds can be a source of major disorder both in the amorphous phase and in the microcrystalline graphitic domains for instance—in the latter via bond-

angle distortion and formation of cross-links between the atomic planes. Interestingly, in spite of a hydrogen loss upon $N^+$ implantation, the graphitic component of the C films decreased. We infer that N would play the same role as H in stabilizing a carbon network against graphitization. In fact, due to its low coordination numbers in the groups stressed above, 2 and 1, and due to its electronegativity being higher than that of C, N can act as a perfect strain-relieving element. A low coordination number gives more freedom for N to connect amorphous regions, and in this way N may stabilize amorphous films against (micro-) crystallization. Moreover, N in the carbon films may stabilize the amorphous phase through breaking the strained C–C bonds and then saturating the broken bonds by forming –C≡N. These chemical effects can explain the amorphicity enhancement in the ii-$CN_x$ films. Besides this, the ballistic processes and the resulting increased defect density play an important role in determining the final structure of the implanted films. A softening of the films can be well explained by such a factor. In turn, the structural damage confers to the irradiated surface a specific structure which improves its friction behaviour.

## 5. Conclusion

We have characterized diamond-like carbon films prepared by r.f. magnetron sputtering and have studied the effects of implanted nitrogen on the electronic structure, the composite microstructure and the chemical states of C in these films.

The films were found to have a two-phase structure: microcrystalline graphitic domains dispersed in an amorphous matrix. The films were hard and of a rigidity index close to that of diamond. $N^+$ implantation induced an amorphization of the graphitic component of the carbon network and at the same time preserved the connectivity of the amorphous phase and its modulus of elasticity. The implanted N atoms bonded to C in various N/C atomic ratios. The latter follows the N concentration in depth and reaches values as high as 1.8. These new chemical bonds can account for the enhanced amorphicity in the implanted films. Ballistic events played a role (i) in the film softening and (ii) in the surface property modifications, which affected the population of the electronic states near the Fermi level and resulted in an improved friction behaviour of the $N^+$-irradiated films.

## Acknowledgments

The authors are grateful to M Bonelli, E Voltolini and M Adami for the ion implantation.

## References

[1] Wood P, Wydeven T and Tsuji O 1995 *Thin Solid Films* **258** 151
[2] Rossi F, Andre B, van Veen A, Mijnarends P E, Schut H, Labohm F, Dunlop H, Delplanke M P and Hubbard K 1994 *J. Mater. Res.* **9** 2440
[3] Sjostrom H, Ivanov I, Johansson M, Hultman L and Sundgren J-E 1994 *Thin Solid Films* **246** 103
[4] Boyd K J, Marton D, Todorov S S, Al-bayati A H, Kulik J, Zuhr R A and Rabalais J B 1995 *J. Vac. Sci. Technol.* A **13** 2110
[5] Fujimoto F and Ogata K 1993 *Japan. J. Appl. Phys.* **32** L420
[6] Gouzman I, Brener R and Hoffman A 1994 *Thin Solid Films* **253** 90
[7] Xin H, Xu W, Shi X, Zhu H, Lin C and Zou S 1995 *Appl. Phys. Lett.* **66** 3290
[8] Ziegler J F 1992 *Handbook of Ion Implantation Technology* ed J F Ziegler (Amsterdam: Elsevier–North-Holland) pp 1–68
[9] Vizkelethy G 1990 *Nucl. Instrum. Methods* **45** 1
[10] Shirley D A 1972 *Phys. Rev.* **55** 4709

[11] Vegh J 1988 *J. Electron Spectrosc. Relat. Phenom.* **46** 411
[12] Seah M P and Smith G C 1990 *Practical Surface Analysis* 2nd edn, vol 1, ed D Briggs and M P Seah (Chichester: Wiley) appendix 1, pp 543–4
[13] *CRC Handbook of Chemistry and Physics* 1987–1988 ed R C Weast (Boca Raton, FL: Chemical Rubber Company Press)
[14] Smith F W 1984 *J. Appl. Phys.* **55** 7664
[15] Savvides N 1986 *J. Appl. Phys.* **59** 4233
[16] Lam N Q and Okamoto P R 1978 *J. Nucl. Mater.* **78** 40 821
[17] Rossi F 1992 *Advanced Techniques for Surface Engineering* ed W Gissler and H A Jehn (Dordrecht: Kluwer Academic) pp 371–97
[18] Holleck H 1986 *J. Vac. Sci. Technol.* A **4** 2661
[19] Marshall D B, Noma T and Evans A G 1982 *J. Am. Ceram. Soc.* **65** C175
[20] Robertson J 1992 *Phys. Rev. Lett.* **68** 220
[21] Lawn B R, Evans A G and Marshall D B 1980 *J. Am. Ceram. Soc.* **63** 574
[22] Lurie P G and Wilson J M 1977 *Surf. Sci.* **65** 476
[23] Briggs D and Riviere J C 1983 *Practical Surface Analysis* ed D Briggs and M P Seah (New York: Wiley) pp 87–139
[24] Weaire D and Thorpe M F 1971 *Phys. Rev.* B **4** 2508
[25] Torng J, Sivertsen J M, Judy J H and Chang C 1990 *J. Mater. Res.* **5** 2490
[26] Kittel C 1971 *Introduction to Solid State Physics* (New York: Wiley)
[27] Galuska A A and Madden H H 1988 *Appl. Surf. Sci.* **32** 253 and references [22] and [18] therein
[28] Gora T, Staley R, Rimdidt J D and Sharma J 1972 *Phys. Rev.* B **5** 2309
[29] McFeely F R, Kowlaczyk S P, Ley L, Cavell R G, Pollak R A and Shirley D A 1974 *Phys. Rev.* B **9** 5268
[30] Tsai H and Bogy D B 1987 *J. Vac. Sci. Technol.* A **5** 3287
[31] Painter G S, Ellis D E and Lubinsky A R 1971 *Phys. Rev.* B **4** 3610
[32] Willis R F, Fitton B and Painter G S 1974 *Phys. Rev. Lett.* B **9** 1926
[33] Khvostov V V, Guseva M B, Babaev V G and Rylova Yu O 1986 *Surf. Sci.* **169** L253
[34] Mansour A and Ugolini D 1993 *Phys. Rev.* B **47** 10 201
[35] Fujimoto F and Ogata K 1993 *Japan. J. Appl. Phys.* **32** L420
[36] Xin H, Xu W, Shi X, Zhu H, Lin C and Zou S 1995 *Appl. Phys. Lett.* **66** 3290
[37] Briggs D and Riviere J C 1983 *Practical Surface Analysis* ed D Briggs and M P Seah (New York: Wiley) pp 359–96
[38] Marletta G, Oliveri C, Ferla G and Pignataro S 1988 *Surf. Interface Anal.* **12** 447
[39] Ricci M, Trinquecoste M, Auguste F, Canet R, Delhaes P, Guimon C, Pfister-Guillouzo G, Nysten B and Issi J P 1993 *J. Mater. Res.* **8** 480
[40] Joannopoulos J D and Cohen M L 1973 *Phys. Rev.* B **7** 2644
[41] Huong P V 1991 *Diamond Relat. Mater.* **1** 33
[42] Yoshikawa M, Katagiri G, Ishida H and Ishitani A 1988 *Solid State Commun.* **66** 1177
[43] Solin S A and Kobliska R 1973 *Proc. 5th Int. Conf. on Amorphous and Liquid Semiconductors (Garmish Partenkirchen, 1973)* ed J Stike and W Brenig (London: Taylor and Francis) pp 1251–8
[44] Nemanich R J, Glass J T, Lucowsky G and Shroder R E 1988 *J. Vac. Sci. Technol.* A **6** 1783
[45] Shayegan M, Dresselhaus M S, Mazurek H and Dresselhaus G 1981 *Phys. Rev.* B **24** 1027